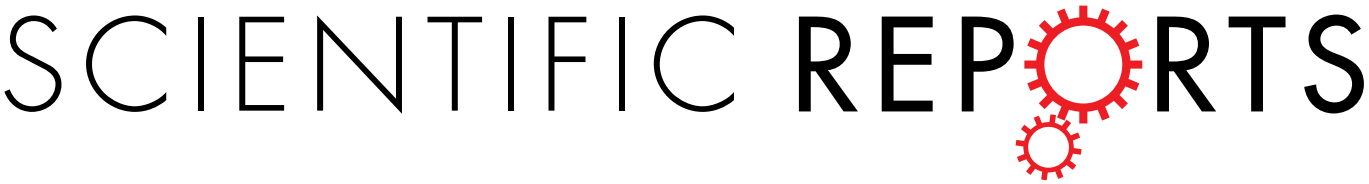

OPEN

Nighttime dissolution in a temperate coastal ocean ecosystem increases under acidification

Received: 28 October 2015
Accepted: 24 February 2016
Published: 18 March 2016

Lester Kwiatkowski[1], Brian Gaylord[2], Tessa Hill[2,3], Jessica Hosfelt[2,3], Kristy J. Kroeker[2,4], Yana Nebuchina[1], Aaron Ninokawa[2], Ann D. Russell[2,3], Emily B. Rivest[2], Marine Sesboüé[1] & Ken Caldeira[1]

Anthropogenic emissions of carbon dioxide (CO_2) are causing ocean acidification, lowering seawater aragonite ($CaCO_3$) saturation state (Ω_{arag}), with potentially substantial impacts on marine ecosystems over the 21st Century. Calcifying organisms have exhibited reduced calcification under lower saturation state conditions in aquaria. However, the *in situ* sensitivity of calcifying ecosystems to future ocean acidification remains unknown. Here we assess the community level sensitivity of calcification to local CO_2-induced acidification caused by natural respiration in an unperturbed, biodiverse, temperate intertidal ecosystem. We find that on hourly timescales nighttime community calcification is strongly influenced by Ω_{arag}, with greater net calcium carbonate dissolution under more acidic conditions. Daytime calcification however, is not detectably affected by Ω_{arag}. If the short-term sensitivity of community calcification to Ω_{arag} is representative of the long-term sensitivity to ocean acidification, nighttime dissolution in these intertidal ecosystems could more than double by 2050, with significant ecological and economic consequences.

The oceanic uptake of CO_2 has increased due to anthropogenic CO_2 emissions[1]. This process, often referred to as 'ocean acidification', has decreased global surface ocean pH by ~0.1 since the preindustrial era[2] and is projected to further decrease pH by 0.07 to 0.33 units by 2100[3]. The ongoing reduction of the calcium carbonate saturation state of seawater, contemporaneous with ocean acidification[4], is likely to affect the ability of many marine calcifiers to form their calcium carbonate shells or skeletons and is projected to have significant impacts on ocean ecosystems on decadal to millennial timescales[5,6].

Calcification rates are a common indicator of individual or ecosystem health[7]. In laboratory manipulations, many calcifying species, including temperate macroalgae[6,8,9] and invertebrates[10,11,12], exhibit reduced rates of calcification in response to a reduction in the seawater saturation state. Consequently, *in situ* observations of the sensitivity of calcifying communities to natural saturation state variability are increasingly valued[13], as they incorporate complex species interactions, and capture the carbonate chemistry conditions to which communities are acclimatised. Such analyses may therefore better represent the community level sensitivity to long-term ocean acidification. Studies have typically focused on sites with volcanic CO_2 seeps that produce strong spatial gradients in calcium carbonate saturation state[13,14]. However, an alternative approach has been applied at sites that are isolated from the open ocean during low tides and can therefore experience large temporal (hourly) variability in calcium carbonate saturation state due to localised photosynthesis and respiration[15,16]. It is this approach that is utilised in this study to investigate the sensitivity of calcifiers to saturation state variability in temperate intertidal ecosystems. The main difference between the two methodologies is that the sensitivity of a community exposed to large short-term variability in carbonate saturation state may differ from that community's sensitivity to ocean acidification which operates over much longer decadal to centennial timescales. As such, greater care is required when making long-term inferences from temporally isolated study sites.

Here, we assess the community level sensitivity of temperate tide pool calcification rates to variability in the calcium carbonate saturation state. Our intertidal study site at Bodega Marine Reserve in Northern California

[1]Department of Global Ecology, Carnegie Institution for Science, 260 Panama Street, Stanford, California, 94305, USA. [2]Bodega Marine Laboratory, University of California at Davis, Bodega Bay, California, 94923, USA. [3]Department of Earth & Planetary Sciences, University of California, Davis, CA 95616, USA. [4]Department of Ecology and Evolutionary Biology, Santa Cruz, California, 95064, USA. Correspondence and requests for materials should be addressed to L.K. (email: lkwiatkowski@carnegiescience.edu)

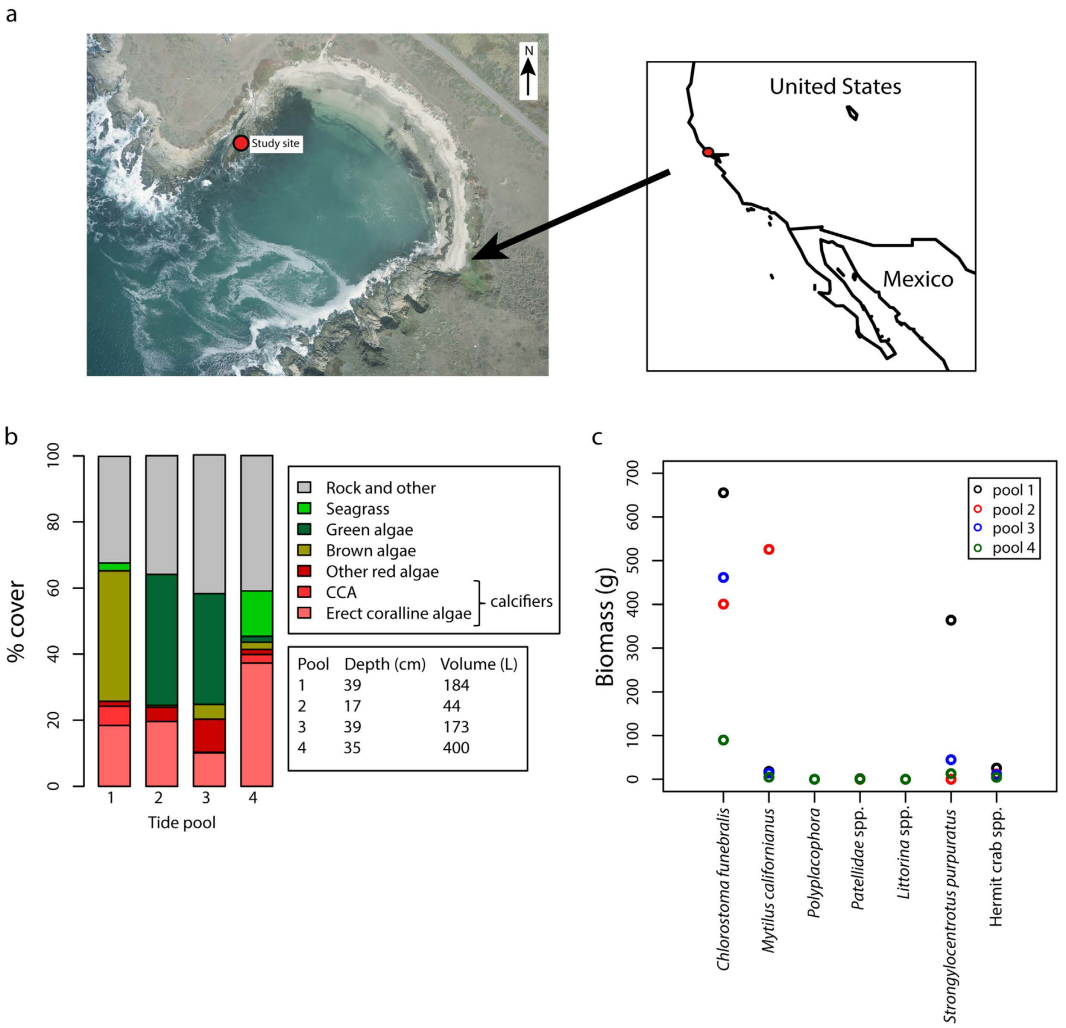

Figure 1. Study site characterisation. (**a**) An aerial photo of Horseshoe Cove, Bodega Marine Reserve, California and the location of the tide pool study site on the Northern California coast (38.3°N, 123.1°W), (**b**) the mean depth, volume and primary producer community cover and (**c**) the invertebrate community in each of the tide pools. The map is produced using R version 3.0.3 software (https://www.r-project.org/).

experiences extreme variation in calcium carbonate saturation state at low tide due to photosynthetic activity and respiration occurring after the time at which the pools become isolated from the open ocean. As photosynthetic activity is largely dependent on temperature and photosynthetically active radiation (PAR), which vary on a diurnal timescale, whereas tide pool isolation is predominantly a function of tidal phase, we were able to separate the influence of calcium carbonate saturation state on calcification from the influence of temperature and PAR. This system therefore provides a unique opportunity to characterise the *in situ* short-timescale sensitivity of tide pool community calcification rates to changes in saturation state.

Results

Tide pool community structure. The mean depths, volumes, and community structure of the pools are given in Fig. 1. Mean pool depth varied from 17 cm to 39 cm while pool volume covered the range 44 L to 400 L. The dominant autotrophic calcifiers in the pools were coralline algae (e.g. *Corallina vancouveriensis* and *Calliarthron* sp.; 10.1–37.3% benthic cover) and crustose coralline algae (CCA; 0–5.8% benthic cover). The tide pool communities included various non-calcifying red algae (*Prionitis* sp. and *Mastocarpus* sp.; 1.5–10% benthic cover), brown algae (e.g. *Fucus vesiculosus*; 0.6–39.5% benthic cover), green algae (*Cladophora* sp. and *Enteromorpha* sp.; 0.04–39.6% benthic cover) and seagrasses (*Phyllospadix torreyi*.; 0.01–13.7% benthic cover). We note that pools also contained a diverse calcifying invertebrate community, including bivalves (i.e., *Mytilus californianus*) and gastropods (i.e., *Chlorostoma funebralis*, *Littorina* spp., *Polyplacophora* spp., and limpets). In the majority of pools, the dominant component of calcifying invertebrate biomass was *Chlorostoma funebralis* (Fig. 1c).

Carbonate chemistry. The carbonate chemistry of seawater in the tide pools varied substantially throughout the day in all pools studied (Fig. 2). Total alkalinity (A_T) and dissolved inorganic carbon (C_T) were highest

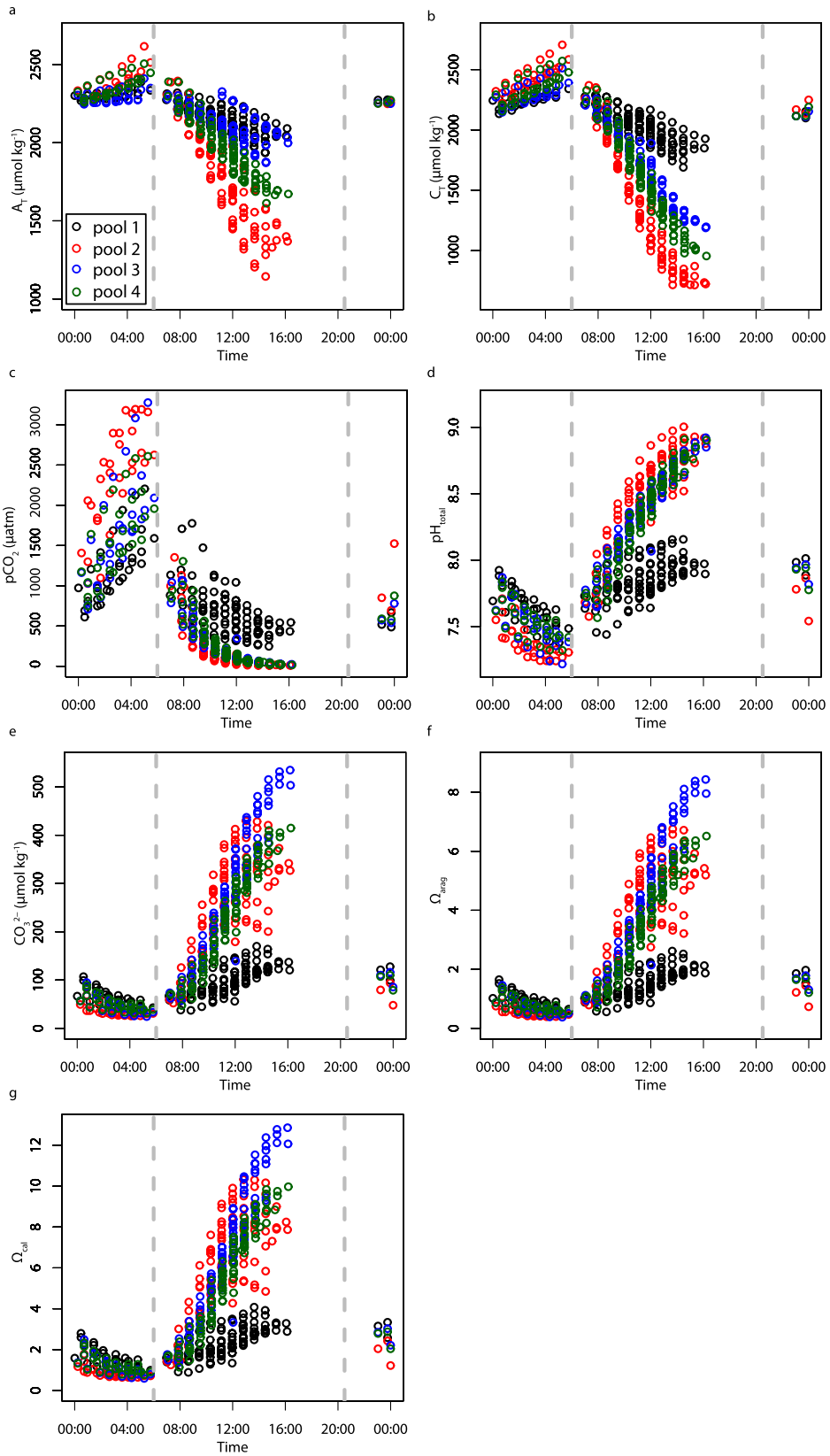

Figure 2. Carbonate chemistry parameters. (**a**) total alkalinity (A_T; μmol kg^{-1}), (**b**) dissolved inorganic carbon (C_T; μmol kg^{-1}), (**c**) pCO_2 (μatm), (**d**) pH, (**e**) CO_3^{2-} concentration (μmol kg^{-1}), (**f**) aragonite saturation state (Ω_{arag}) and (g) calcite saturation state (Ω_{cal}) against time of day for all experimental time periods in each of the tide pools. Dashed grey lines show the approximate times of sunrise and sunset. Daytime data were collected in 2014 and nighttime data in 2015.

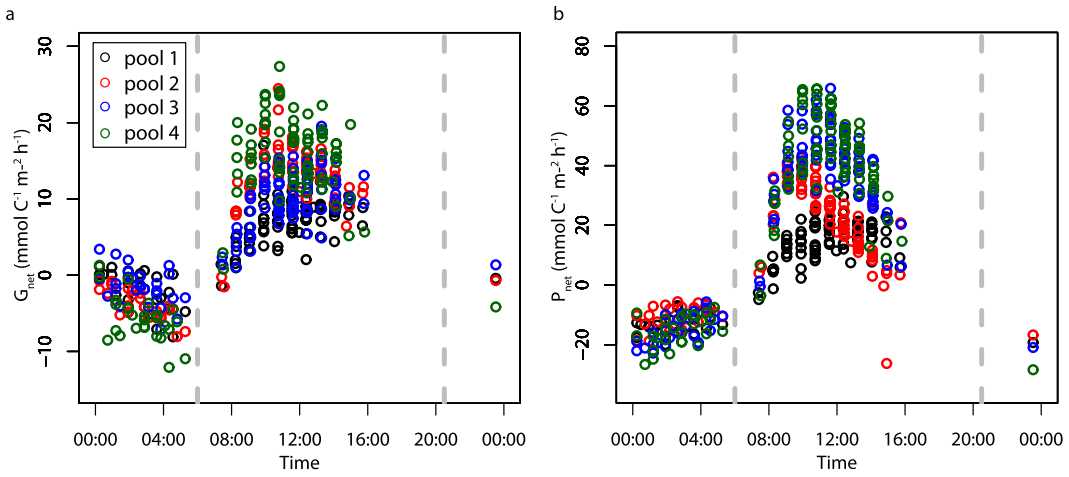

Figure 3. Temporal cycles in community calcification (G_{net}) and production (P_{net}). (**a**) G_{net} (mmol C^{-1} m^{-2} h^{-1}) and (**b**) P_{net} (mmol C^{-1} m^{-2} h^{-1}) against time of day in each of the tide pools. Dashed grey lines show the approximate times of sunrise and sunset. Daytime data were collected in 2014 and nighttime data in 2015.

before sunrise (maximum value of $A_T = 2616$ µmol kg^{-1}; $C_T = 2512$ µmol kg^{-1}) and decreased through the course of the day to minimum values in the late afternoon (minimum value of $A_T = 1144$ µmol kg^{-1}; $C_T = 715$ µmol kg^{-1}). The pCO_2 showed similar declines, with a peak pre-sunrise value of 3276µatm and a minimum value of <10 µatm by mid-to-late afternoon. The pH, CO_3^{2-} and Ω_{arag} all show large concurrent decreases through the night and increases during the day, with pH increasing from a minimum value before sunrise of 7.22 to a maximum late afternoon value of 9.00, and Ω_{arag} increasing through the day from a minimum value of 0.38 before sunrise to a maximum of 8.43. As discussed in greater detail below, the variation in carbonate chemistry parameters can be largely attributed to patterns of calcification, net primary production and changes in tide pool temperature.

While all four tide pools had broadly similar directional trends in carbonate chemistry parameters throughout the day, the magnitude of these trends shows large differences among pools. These differences are due to tide pool depth and the relative abundance of calcifying and photosynthesising taxa, in addition to the relative exposure of pools to incoming solar radiation. Pool 1, in particular, shows diel ranges in carbonate chemistry parameters of a much lower magnitude than the other pools (Fig. 2). Greater shading from incoming solar radiation and therefore lower pool temperature and PAR levels in Pool 1 may have enhanced the stability of its carbonate chemistry. The magnitude of carbonate chemistry changes in Pools 2, 3 and 4 seems to largely reflect pool depth, with shallower pools characterised by more substrate per pool volume (and thus greater benthic biomass per volume) exhibiting the largest daily reductions in A_T and C_T (Fig. 2).

Daytime calcification. Rates of daytime calcification are predominately positive, indicating net community calcification during daylight hours. Net community calcification (G_{net}) shows similar diel trends to net community production (P_{net}), with peak rates typically occurring between 11:00 and 13:00 (Fig. 3).

In all pools, G_{net} is linearly correlated with P_{net} ($p < 0.05$). G_{net} is linearly correlated to PAR, achieving statistical significance ($p < 0.01$) in all pools except for Pool 4 ($p = 0.11$). This is likely an artefact of the fewer measurements made at low light levels in Pool 4. While linearly correlated, the data suggest that the relationship between G_{net} and PAR can be better described by a Michaelis-Menten function with the positive influence of PAR on G_{net} saturating at PAR values >1000 µmol m^{-2} s^{-1} (Supplementary Fig. S4). G_{net} is linearly correlated to temperature ($p < 0.05$) and Ω_{arag} ($p < 0.05$) in all pools with the exception of Pool 4.

P_{net}, PAR, and a Gaussian function of temperature (T_f) explain 33–71% of the variation in daytime G_{net} in the tide pools studied (Table 1). Ω_{arag} offers no additional explanatory power in the prediction of daytime G_{net} for any of the tide pools, if variation in P_{net}, PAR, and T_f is taken into account (Table 1).

Nighttime calcification. Nighttime community calcification (G_{net}) is found to be strongly influenced by Ω_{arag}, with higher nighttime G_{net} at higher Ω_{arag} values in all tide pools. This is in contrast to the Ω_{arag} insensitivity described for daytime G_{net}. Nighttime G_{net} typically occurs at lower Ω_{arag} values (0.38–2.06) than those present during the day (0.56–8.43), and is predominately negative, indicating net $CaCO_3$ dissolution (Fig. 3). Ω_{arag} can explain 28–53% of the variability in nighttime calcification rates (Fig. 4a). Regression analyses indicate that the transition from net calcification to net dissolution occurs at Ω_{arag} values of 1.52, 1.05, 1.05 and 1.73 for Pools 1–4 respectively (Fig. 4a).

In the absence of other potential explanatory variables temperature was found to explain 20–45% of variability in nighttime G_{net} in 3 of the 4 pools (Fig. S6). P_{net} is found to only explain 21% of the variability in nighttime G_{net} in Pool 2 (Fig. S6) and none of the variability in nighttime G_{net} in the other tide pools. P_{net} is not present in the optimal nighttime model of Pool 2 (Table 1).

The dominant driver of nighttime G_{net} variability is Ω_{arag}, with greater dissolution rates at lower values. Ω_{arag} is the only explanatory variable in the optimal model of calcification in each pool (Table 1) and explains 28 ± 9% of additional variability in nighttime G_{net} that is unaccounted for by P_{net} and T_f. In total 47–62% of the variability in

Pool	Variable	Coefficient	Standard error	R^2
Daytime Calcification				
1	PAR_{mm}	25.74	4.00	0.34
2	P_{net}	0.12	0.02	0.71
	PAR_{mm}	8.62	1.60	
	T_f	0.55	0.11	
3	PAR_{mm}	25.43	4.16	0.33
4	P_{net}	0.22	0.03	0.45
Nighttime Calcification				
1	Ω_{arag}	6.16	1.32	0.47
	P_{net}	0.37	0.12	
2	Ω_{arag}	7.91	1.45	0.53
3	Ω_{arag}	4.17	1.11	0.62
	T_f	0.60	0.22	
4	Ω_{arag}	8.70	1.66	0.53
	P_{net}	0.26	0.08	

Table 1. Statistical model parameter estimates for daytime and nighttime calcification. The optimal models of daytime and nighttime net calcification (G_{net}) in each of the tide pools. During the night Ω_{arag} is the only potential explanatory variable in the optimal model of each tide pool. However during the day Ω_{arag} is found to offer no additional explanatory power in any of the tide pools. In each model all explanatory variables are significant at the $p < 0.01$ level.

nighttime G_{net} can be explained by Ω_{arag}, P_{net} and T_f. Ω_{arag} has a coefficient of 6.16 ± 1.32, 7.91 ± 1.45 4.17 ± 1.11, and 8.70 ± 1.66 for Pools 1–4 respectively. As such, the Ω_{arag} sensitivity of nighttime calcification is broadly indistinguishable between tide pools although Pool 3 is less sensitive to Ω_{arag} variability than Pools 2 and 4.

Discussion

The finding that Ω_{arag} offers no additional explanatory power in the prediction of daytime G_{net}, if variation in P_{net}, PAR, and temperature is taken into account (Table 1), suggests that at least in the short-term, daytime net calcification rates of intertidal communities are resilient to a very broad range of Ω_{arag} values (0.56–8.43). Daytime calcification rates could exhibit some dependency on Ω_{arag} as has been shown for individual species in laboratory manipulations that encompass a similar Ω_{arag} range[10,12,17] but due to multicollinearity between Ω_{arag} and other potential explanatory variables such as PAR, this dependence may not be detectable *in situ*[18,19]. Such dependency however is highly unlikely given that the multicollinearity between explanatory variables is weak in our study (Supplementary Tables S1 and S2).

The positive correlations between G_{net} and P_{net} during the daytime imply that calcification and photosynthesis are intimately linked in these tide pools. This suggests that photosynthesis could enhance calcification processes during daylight hours[20,21] and promote greater calcification resilience to variability in Ω_{arag}. In the intertidal communities studied here, photosynthetic calcifiers (i.e., calcifying algae) may have a larger influence on carbonate chemistry dynamics than non-photosynthetic calcifying species, such as molluscs, during daylight hours. While we did not assess the extent to which individual taxa contribute to net community calcification in the tide pools, our results allow for predictions about the vulnerability of net daytime community calcification to variability in Ω_{arag} across a range of community compositions.

As shown in Fig. 4b, the decline of global mean Ω_{arag} as projected by an ensemble of current-generation Earth System Models, is highly dependent on the economic and environmental pathway taken. Under a business-as-usual scenario (RCP 8.5), global mean Ω_{arag} is projected to decline by 1.32 by the year 2100, relative to global mean Ω_{arag} in 1990–2000. Even under an extremely ambitious pathway aimed to limit global mean temperature rise to 2 °C (RCP 2.6), which assumes full participation in emission reductions by all countries, and the possibility of negative emissions[22], Ω_{arag} is still expected to decline by up to 0.33 throughout the 21st Century, relative to 1990–2000 mean Ω_{arag}. Although the extent to which global declines in Ω_{arag} are reflected in intertidal zones will vary regionally and be mediated by local processes[23], it is apparent that projected declines in Ω_{arag} are considerably smaller than our measured diel variability due to photosynthesis and respiration. The impact of ocean acidification in intertidal ecosystems will therefore be a consequence of the sensitivity of communities already exposed to a wide Ω_{arag} range experiencing a relatively smaller decline in mean background Ω_{arag}[24].

The statistical models derived for nighttime calcification all contain Ω_{arag}, with P_{net} and a Gaussian function of temperature (T_f) found to offer additional explanatory power in certain tide pools. Ω_{arag} coefficients in these models are between 4.17 ± 1.11 and 8.70 ± 1.66 depending on the tide pool. Therefore, a decline in background Ω_{arag} values of 0.5, which is highly likely by 2050 under even optimistic scenarios of future climate change (Fig. 4b)[4,25], would reduce nighttime calcification (increase nighttime dissolution) by approximately 2.09–4.35 mmol C^{-1} m^{-2} h^{-1}. Given that we measure mean nighttime calcification rates of -3.24 mmol C^{-1} m^{-2} h^{-1}, this represents a decline in net community calcification of approximately 65–134% based on the statistical relationships derived in our experiment. It should be noted that our *in-situ* methodology does not distinguish between organism and sediment

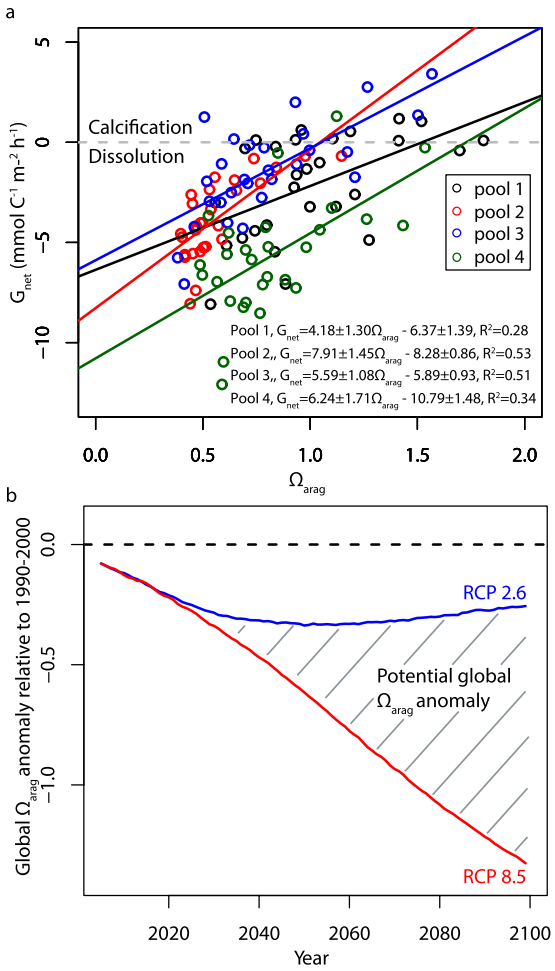

Figure 4. Nighttime community calcification and Ω_{arag} sensitivities/projections. (**a**) Nighttime G_{net} (mmol C^{-1} m^{-2} h^{-1}) against aragonite saturation state (Ω_{arag}) in each of the tide pools. Regression lines are significant at the $p < 0.05$ level. (**b**) Coupled Model Intercomparison Project Phase 5 (CMIP5) global Ω_{arag} anomalies relative to 1990–2000 mean values for the Representative Concentration Pathways 2.6 (RCP 2.6; blue) and 8.5 (RCP 8.5; red). Ω_{arag} anomalies are multimodel ensemble mean values calculated from 8 CMIP5 models with fully coupled ocean biogeochemistry schemes. RCP 2.6 and RCP 8.5 respectively represent the most extreme mitigation and business-as-usual RCP scenarios conducted in CMIP5.

$CaCO_3$ dissolution. Therefore additional controlled lab and mesocosm studies are required to isolate the biotic community sensitivity to Ω_{arag} variability and demonstrate that it does not significantly differ from the aggregate community sensitivity observed *in situ*.

Our estimates of the sensitivity of intertidal communities to Ω_{arag} responses recorded on hourly time scales only partially reflect the potential long-term response of ecosystems to decadal to millennial scale changes brought about by anthropogenic carbon dioxide emissions. Indeed, the sensitivity of intertidal organisms to Ω_{arag} in manipulative experiments has been shown to exhibit dependence on experimental duration[26,27] and therefore the short-term Ω_{arag} sensitivity of the communities characterised here may differ from their long-term sensitivity to ocean acidification. Moreover, the overall impacts of ocean acidification and declining Ω_{arag} on temperate calcifiers will be more diverse and extend beyond the processes we evaluated, including potential impacts on survival and reproduction[7]. Nonetheless, if the short-term sensitivity of community calcification to Ω_{arag} conditions ranging from 0.38 to 8.43 described here is representative of the long-term sensitivity of these intertidal communities to ocean acidification, then one would expect daytime net calcification rates to be relatively resilient to future Ω_{arag} declines. Nighttime net calcification rates however, would be expected to decline, reducing the long-term community calcification of these ecosystems, with important ecological and economic ramifications.

Materials and Methods

Oceanographic and geochemical measurements. Our study site consisted of 4 rocky tide pools located in Horseshoe Cove, Bodega Marine Reserve, California (38.3°N, 123.1°W; Fig. 1). Over 5 sampling periods in April, May and June 2014, and May and June 2015, instruments were deployed in each of the tide pools over low tide periods (~7 hours, during which the pools were isolated from the open ocean). The sampling periods in 2014 occurred during daylight hours, while the sampling periods in 2015 occurred at night. The influence of interannual variability on comparisons between the 2014 and 2015 datasets is assumed to be minimal. This is

supported by the agreement between 2014 and 2015 carbonate chemistry measurements in the crepuscular periods. Monthly differences between the PAR levels at a given time of day were minimal once periods with overcast conditions are taken account of. We utilised conductivity-temperature-depth sensors (CTDs; YSI model 6600 and 6920) to measure pressure, temperature, conductivity, pH, and oxygen at intervals of 2 minutes. When oxygen levels were high and interfered with conductivity measurements, salinity values were estimated from contemporaneous measurements in other tide pools. Water pumps attached to CTDs were used to take 1 L bottle samples every 50 minutes over the course of instrument deployment for discrete geochemical analyses (below). Seawater samples were analysed immediately for alkalinity and pH and preserved with $HgCl_2$ for dissolved inorganic carbon (C_T) analysis.

In total, 566 seawater samples were analysed for total alkalinity (A_T), pH, dissolved inorganic carbon (C_T and nutrients ($NO_2^- + NO_3^-$ and $NH_3 + NH_4^+$). A_T was measured using a Metrohm 855 autotitrator. Three replicates of each sample were run, and the mean value of the two closest replicates was used ($<2\,\mu mol\,kg^{-1}$ (1SD) instrument precision). Titrant was standardised using reference material supplied by the Dickson Lab (Batch 141). The pH and O_2 values measured via CTD were calibrated using spectrophotometric pH measurements and Winkler titrations, respectively, conducted according to best practices[28] on discrete water samples. C_T was measured by infrared adsorption via a LICOR7000 CO_2/H_2O analyser coupled with a custom-made sample delivery system built by Stanford University's Stable Isotope Laboratory ($<2\,\mu mol\,kg^{-1}$ (1SD) instrument precision). Nutrients were measured photometrically using a WestCo SmartChem 200 discrete analyser ($\sim 0.05\,\mu mol\,L^{-1}$ instrument precision). The pCO_2, CO_3^{2-} and aragonite saturation state (Ω_{arag}) values were calculated with A_T and C_T for 2014 data, and A_T and pH for 2015 data, using the CO2SYS program[29]. The K_1 and K_2 constants of Mehrbach *et al.*[30] refit by Dickson and Millero[31] were utilised, and total boron was calculated using the B/chlorinity ratio of Uppstrom 1974[32].

Photosynthetically-active radiation (PAR) data were provided by the Bodega Ocean Observing Node, University of California, Bodega Marine Laboratory (http://bml.ucdavis.edu/boon/index.html). This record is measured within 100 m of the tide pools and is representative of local conditions. However, we note that local topography, water depth, and turbidity are additional influences on the direct PAR that tide pool communities received during the sample collection periods.

Quantification of tide pool volume and community composition. Tide pool volumes were measured by draining each of the 4 tide pools and measuring the volume of drained water. The species composition and community structure of each pool was measured by overlaying a flexible mesh net with 10×10cm grid cells over the bottom of the emptied tide pool. The percent cover of all autotropic species and key functional groups was estimated on a 0 to 4 scale in each grid cell, with 0 denoting absence, 1 = 25%, 2 = 50%, 3 = 75%, and 4 = 100% cover for each taxa. The numerical values were then summed to estimate the total percent cover of each taxa within a tide pool. Invertebrate biomass values were estimated by weighing a representative sample of each taxa.

Net community calcification and production. Net community calcification (G_{net}; mmol $C^{-1}\,m^{-2}\,h^{-1}$) was calculated in each tide pool using the salinity-normalised alkalinity anomaly method[28]:

$$G_{net} = \frac{-0.5\,\Delta A_T\,d\rho}{\Delta t} \tag{1}$$

where ΔA_T is the change in salinity-normalised A_T ($\mu mol\,kg^{-1}$), d is the mean tide pool depth (m), ρ is the density of sea water ($kg\,m^{-3}$)[33] and Δt is the time period (h). Net community production (photosynthesis minus respiration; P_{net}; mmol $C^{-1}\,m^{-2}\,h^{-1}$) is calculated as:

$$P_{net} = \frac{-\Delta C_T\,d\,\rho}{\Delta t} - G_{net} + F_{CO_2} \tag{2}$$

where ΔC_T is the change in salinity normalised C_T ($\mu mol\,kg^{-1}$) and F_{CO_2} ($\mu mol\,kg^{-1}\,m^{-2}\,h^{-1}$) is the air-sea flux of CO_2 calculated using the wind speed-dependent gas transfer function of Ho *et al.* 2006[34], the temperature and salinity dependent solubility of CO_2 according to Weiss 1974[35] and an atmospheric CO_2 concentration of 401 ppm and 403 ppm for the 2014 and 2015 sampling periods respectively (the NOAA/ESRL Mauna Loa mean CO_2 concentration over the sampling periods). Wind speed data were provided by the Bodega Ocean Observing Node, University of California, Bodega Marine Laboratory.

Statistical modelling. Linear least square regression models were used to determine the influence of P_{net}, PAR, temperature, and Ω_{arag} on the rate of community calcification (G_{net}). Such an approach has been previously adopted in tropical environments (e.g. [16,36]). Statistical issues involving multicollinearity between potential explanatory variables was assessed using Variance Inflation Factors (VIFs), which were all less than 6.5 (Supplementary Table S1). Model selection was based on minimising model AIC values with PAR-dependency assumed to follow a Michaelis-Menten function[20] and temperature dependency assumed to follow a Gaussian function[37] (Supplementary Fig. S4). The use of these functions as opposed to linear PAR and temperature relationships improved the explanatory power of models across tide pools. Thus, for each tide pool:

$$G_{net} = \beta_0 + \beta_1(P_{net}) + \beta_2(PAR_{mm}) + \beta_3(T_f) + \beta_4(\Omega_{arag}) + \varepsilon \tag{3}$$

where Ω_{arag} is the mean of the omega aragonite values measured in two consecutive sampling times, PAR_{mm} is a Michaelis-Menten function of the mean PAR between two consecutive sampling times and T_f is a Gaussian

function of the mean temperature between two consecutive sampling times. PAR_{nm} and T_f are derived separately for each tide pool from G_{net}-PAR and G_{net}-temperature relationships respectively (Supplementary Fig. S4). Note that equation 3 simplifies to the following for statistical models of nighttime calcification rates:

$$G_{net} = \beta_0 + \beta_1(P_{net}) + \beta_2(T_f) + \beta_3(\Omega_{arag}) + \varepsilon \quad (4)$$

Ω_{arag} projections. Coupled Model Intercomparison Project Phase 5 (CMIP5) global mean Ω_{arag} values are 2005–2100 annual anomalies calculated relative to the 1990–2000 mean values of the respective model. Values are GLobal Ocean Data Analysis Project (GLODAP)[38], corrected and averaged across a multi-model ensemble of 8 CMIP5 Earth System Models which ran fully coupled ocean biogeochemistry schemes (CanESM2, GFDL-ESM2G, GFDL-ESM2M, IPSL-CM5A-LR, IPSL-CM5A-MR, MIROC-ESM, MPI-ESM-LR, MPI-ESM-MR). Ω_{arag} anomalies are given for the Representative Concentration Pathways 2.6 and 8.5[39]. RCP 2.6 and RCP 8.5 respectively represent the most extreme mitigation and business-as-usual RCP scenarios conducted in CMIP5 and are therefore considered to encompass the range of future potential Ω_{arag} values.

References

1. Doney, S. C., Fabry, V. J., Feely, R. A. & Kleypas, J. A. Ocean Acidification: The Other CO_2 Problem. *Annu. Rev. Mar. Sci.* **1,** 169–192 (2009).
2. Caldeira, K. & Wickett, M. E. Oceanography: Anthropogenic carbon and ocean pH. *Nature* **425,** 365–365 (2003).
3. Bopp, L. *et al.* Multiple stressors of ocean ecosystems in the 21st century: projections with CMIP5 models. *Biogeosciences* **10,** 6225–6245 (2013).
4. Ricke, K. L., Orr, J. C., Schneider, K. & Caldeira, K. Risks to coral reefs from ocean carbonate chemistry changes in recent earth system model projections. *Environ. Res. Lett.* **8,** 034003 (2013).
5. Orr, J. C. *et al.* Anthropogenic ocean acidification over the twenty-first century and its impact on calcifying organisms. *Nature* **437,** 681–686 (2005).
6. Anthony, K. R. N., Kline, D. I., Diaz-Pulido, G., Dove, S. & Hoegh-Guldberg, O. Ocean acidification causes bleaching and productivity loss in coral reef builders. *Proc. Natl. Acad. Sci.* **105,** 17442–17446 (2008).
7. Kroeker, K. J. *et al.* Impacts of ocean acidification on marine organisms: quantifying sensitivities and interaction with warming. *Glob. Change Biol.* **19,** 1884–1896 (2013).
8. Gao, K. *et al.* Calcification in the articulated coralline alga Corallina pilulifera, with special reference to the effect of elevated CO_2 concentration. *Mar. Biol.* **117,** 129–132 (1993).
9. Jokiel, P. L. *et al.* Ocean acidification and calcifying reef organisms: a mesocosm investigation. *Coral Reefs* **27,** 473–483 (2008).
10. Gazeau, F. *et al.* Impacts of ocean acidification on marine shelled molluscs. *Mar. Biol.* **160,** 2207–2245 (2013).
11. Waldbusser, G. G. *et al.* A developmental and energetic basis linking larval oyster shell formation to acidification sensitivity. *Geophys. Res. Lett.* **40,** 2171–2176 (2013).
12. Waldbusser, G. G. *et al.* Saturation-state sensitivity of marine bivalve larvae to ocean acidification. *Nat. Clim. Change* **5,** 273–280 (2015).
13. Hall-Spencer, J. M. *et al.* Volcanic carbon dioxide vents show ecosystem effects of ocean acidification. *Nature* **454,** 96–99 (2008).
14. Fabricius, K. E. *et al.* Losers and winners in coral reefs acclimatized to elevated carbon dioxide concentrations. *Nat. Clim. Change* **1,** 165–169 (2011).
15. Silverman, J. *et al.* Carbon turnover rates in the One Tree Island reef: A 40-year perspective. *J. Geophys. Res.* **117** (2012).
16. Shaw, E. C., Phinn, S. R., Tilbrook, B. & Steven, A. Natural *in situ* relationships suggest coral reef calcium carbonate production will decline with ocean acidification. *Limnol. Oceanogr.* **60,** 777–788 (2015).
17. Waldbusser, G. G., Bergschneider, H. & Green, M. A. Size-dependent pH effect on calcification in post-larval hard clam Mercenaria spp. *Mar. Ecol. Prog. Ser.* **417,** 171–182 (2010).
18. Andersson, A. J. & Gledhill, D. Ocean Acidification and Coral Reefs: Effects on Breakdown, Dissolution, and Net Ecosystem Calcification. *Annu. Rev. Mar. Sci.* **5,** 321–348 (2013).
19. Jokiel, P. L., Jury, C. P. & Rodgers, K. S. Coral-algae metabolism and diurnal changes in the CO_2-carbonate system of bulk sea water. *PeerJ* **2,** e378 (2014).
20. Marubini, F., Barnett, H., Langdon, C. & Atkinson, M. J. Dependence of calcification on light and carbonate ion concentration for the hermatypic coral Porites compressa. *Mar. Ecol. Prog. Ser.* **220,** 153–162 (2001).
21. Langdon, C. *et al.* Effect of calcium carbonate saturation state on the calcification rate of an experimental coral reef. *Glob. Biogeochem. Cycles* **14,** 639–654 (2000).
22. Jones, C. *et al.* Twenty-First-Century Compatible CO_2 Emissions and Airborne Fraction Simulated by CMIP5 Earth System Models under Four Representative Concentration Pathways. *J. Clim.* **26,** 4398–4413 (2013).
23. Andersson, A. J., Yeakel, K. L., Bates, N. R. & de Putron, S. J. Partial offsets in ocean acidification from changing coral reef biogeochemistry. *Nat. Clim. Change* **4,** 56–61 (2014).
24. Gaylord, B. *et al.* Ocean acidification through the lens of ecological theory. *Ecology* **96,** 3–15 (2014).
25. Kwiatkowski, L., Cox, P., Halloran, P. R., Mumby, P. J. & Wiltshire, A. J. Coral bleaching under unconventional scenarios of climate warming and ocean acidification. *Nat. Clim. Change* **5,** 777–781 (2015).
26. Ragazzola, F. *et al.* Ocean acidification weakens the structural integrity of coralline algae. *Glob. Change Biol.* **18,** 2804–2812 (2012).
27. Ragazzola, F. *et al.* Phenotypic plasticity of coralline algae in a High CO_2 world. *Ecol. Evol.* **3,** 3436–3446 (2013).
28. Riebesell, U., Fabry, V. J., Hansson, L. & Gattuso, J.-P. *Guide to best practices for ocean acidification research and data reporting*. 260 (Publications Office of the European Union, 2010).
29. Lewis, E. & Wallace, D. W. R. Program Developed for CO_2 System Calculations. (1998).
30. Mehrbach, C., Culberson, C. H., Hawley, J. E. & Pytkowicx, R. M. Measurement of the apparent dissociation constants of carbonic acid in seawater at atmospheric pressure. *Limnol. Oceanogr.* **18,** 897–907 (1973).
31. Dickson, A. G. & Millero, F. J. A comparison of the equilibrium constants for the dissociation of carbonic acid in seawater media. *Deep Sea Res. Part Oceanogr. Res. Pap.* **34,** 1733–1743 (1987).
32. Uppström, L. R. The boron/chlorinity ratio of deep-sea water from the Pacific Ocean. *Deep Sea Res. Oceanogr. Abstr.* **21,** 161–162 (1974).
33. Millero, F. J. & Poisson, A. International one-atmosphere equation of state of seawater. *Deep Sea Res. Part Oceanogr. Res. Pap.* **28,** 625–629 (1981).
34. Ho, D. T. *et al.* Measurements of air-sea gas exchange at high wind speeds in the Southern Ocean: Implications for global parameterizations. *Geophys. Res. Lett.* **33,** L16611 (2006).
35. Weiss, R. F. Carbon dioxide in water and seawater: the solubility of a non-ideal gas. *Mar. Chem.* **2,** 203–215 (1974).

36. Albright, R., Benthuysen, J., Cantin, N., Caldeira, K. & Anthony, K. Coral reef metabolism and carbon chemistry dynamics of a coral reef flat. *Geophys. Res. Lett.* **42,** 2015GL063488 (2015).
37. Marshall, A. T. & Clode, P. Calcification rate and the effect of temperature in a zooxanthellate and an azooxanthellate scleractinian reef coral. *Coral Reefs* **23,** 218–224 (2004).
38. Key, R. M. *et al.* A global ocean carbon climatology: Results from Global Data Analysis Project (GLODAP). *Glob. Biogeochem. Cycles* **18,** GB4031 (2004).
39. Vuuren, D. *et al.* The representative concentration pathways: an overview. *Clim. Change* **109,** 5–31 (2011).

Acknowledgements

We wish to thank S. Shayegh, Brittany Jellison and D. Ross for fieldwork assistance, J. Orr for assistance with data processing, D. Mucciarone and D. Koweek for assistance with DIC measurements and E. Sanford and R. Albright for helpful insight. This work was funded by the Carnegie Institution for Science, UC Multicampus Research Initiatives and Programs and National Science Foundation (OCE 1220648 and OCE 1255194).

Author Contributions

L.K., K.C., B.G. and T.H. conceived and designed the experiment. L.K., J.H., K.J.K., Y.N., A.N., A.R., E.B.R. and M.S. conducted sample analysis. All authors contributed to the manuscript text.

Additional Information

Supplementary information accompanies this paper at http://www.nature.com/srep

Competing financial interests: The authors declare no competing financial interests.

How to cite this article: Kwiatkowski, L. *et al.* Nighttime dissolution in a temperate coastal ocean ecosystem increases under acidification. *Sci. Rep.* **6**, 22984; doi: 10.1038/srep22984 (2016).